

Electronic Supplementary Information

Controlling polymorphism in molecular cocrystals by variable temperature ball milling

Kevin Linberg^[a,b], Bettina Röder^[a], Dominik Al-Sabbagh^[a], Franziska Emmerling^{[a,b]*}, and Adam A. L. Michalchuk^{[a]*}

[a] Kevin Linberg, Röder Bettina, PD Dr Franziska Emmerling and Dr Adam A. L. Michalchuk
Bundesanstalt für Materialforschung und -prüfung (BAM)
Richard-Willstätter-Strasse 11, 12489 Berlin (Germany)
E-mail: adam.michalchuk@bam.de; franziska.emmerling@bam.de

[b] Kevin Linberg, PD Dr. Franziska Emmerling
Department of Chemistry, Humboldt-Universität zu Berlin
Brook-Taylor-Strasse 2, 12489 Berlin (Germany)

CONTENTS

S1 Thermally Controlled Milling Jar	2
S2 Thermodynamic Stability of Cocrystal Polymorphs	3
S3 Quantitative Phase Analysis of Mechanochemically Prepared Powders	5
S4 Time-Resolved In Situ (TRIS) XRPD.....	11
S5 Ball Milling Experiments at Elevated Temperature	12
S6 References.....	15

S1 THERMALLY CONTROLLED MILLING JAR

The heating device comprises an aluminium heating jacket which holds the milling jar and is surrounded by an external insulating polymer jacket. The aluminium jacket is heated by a heater from a 3D Printer (UT 24V 40W J-Head Hotend Heater Cartridge), and the temperature of the milling jar is monitored by a PT 100 temperature sensor located in the aluminium heating element. The whole heating device is thermally insulated by a jacket made of PEEK, manufactured with the CreatBot F430 3D printer. The heating cartridge is embedded in the heating element. The aluminium ensures fast, even heat distribution over the entire grinding jar. Complete technical details are given in Figure S1.

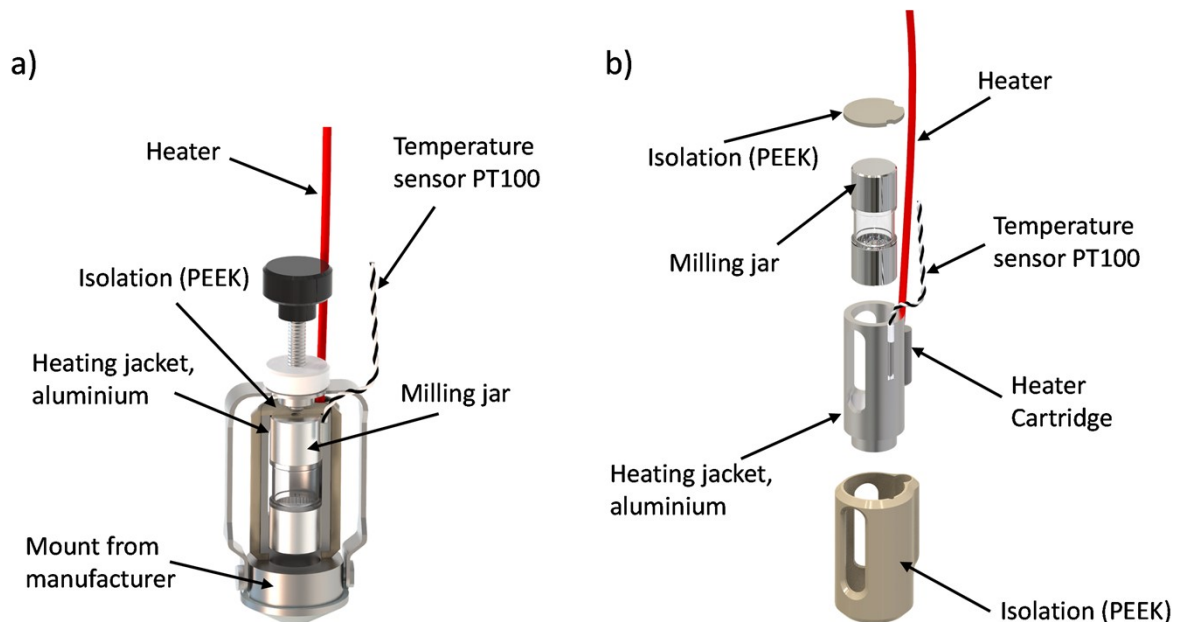


Figure S1 | Schematic representation of the heating set-up developed for our three-piece milling jars¹ for use with the Fritsch P23 Pulverisette mill. The set-up is shown (a) as constructed, and (b) deconstructed, for visibility.

S1.1 THERMOMETER PT100 (RESISTANCE THERMOMETER) | A PT100 resistance thermometer is a temperature sensor that can be used to measure and process temperatures. The PT100 module is connected via a two-wire cable. Since cables and terminals also have electrical resistance, this resistance must be considered in the measurements. For this reason, the measured value(s) of the Eliwell temperature controller was compared with the measured value of the Omega data logger. A cap made of PEEK, printed with the 3D printer, lies between the grinding jar holder and the pressure screw of the grinding jar clamp, and prevents heat loss. The cap also serves as a pressure disc to fix the grinding jar in the heating system. The temperature is monitored and controlled with the aid of the Eliwell 915 two-point temperature controller (Eliwell IC+ 915 12V 8A TCJ/K PT 100).

S1.2 TEMPERATURE CONTROLLER | The IC 915 series temperature controllers are two-stage electronic devices, for controlling temperature, relative humidity, and pressure. Two-point controllers (also 2-point controllers) are simple controllers. They only know two states "On" means heating and "Off" means not heating. Thus, the controller switches off the output when the actual value exceeds a previously set point. If it falls below this point, the controllers switch the output on again. The Eliwell temperature controller has been programmed to 50°C. The power supply for the UT 24V 40W J-Head Hotend Heater was performed with 12 V and was provided by the laboratory power supply unit, Basetech BT-305, adjustable 0 - 30 V/DC 0 - 5 A 150 W. The entire system (insulation, heating mantle, grinding jar) needs a certain time (approx. 20 min) as a warm-up phase. Then the grinding bowl holder has reached a uniform temperature. The overshoot during the warm-up phase is more than 3 K and can be reduced to ± 1.5 K after the desired temperature has been reached by reducing the current supply to 8 V.

S2 THERMODYNAMIC STABILITY OF COCRYSTAL POLYMORPHS

We note that there is a difference between simulated and experimental PXRD profiles from **Form I**, which is due to the measurement temperatures. While the simulated data for **Form I** was collected at 153 K², our data was measured at room temperature. By taking thermal expansion into account, a good agreement of simulated and measured PXRD is achieved, Figure S2.1.

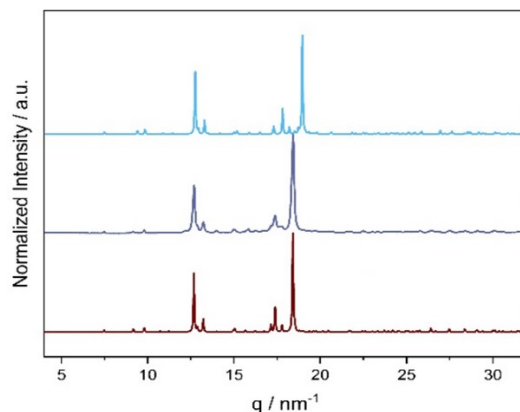


Figure S2.1 | Comparison of **Form I** with simulation from the Literature² (top), RT measurement (middle) and simulation after Rietveld refinement (bottom). We note the offset between simulated and experimental PXRD profiles is the result of measurement temperatures. While simulated data for **Form I** were collected at 153 K², our data were collected at room temperature. By accounting for thermal expansion, a good quality Rietveld refinement is achieved.

Form II transformed into **Form I** over time, Figure S2.2. A complete transformation to **Form I** is detected after 4 days.

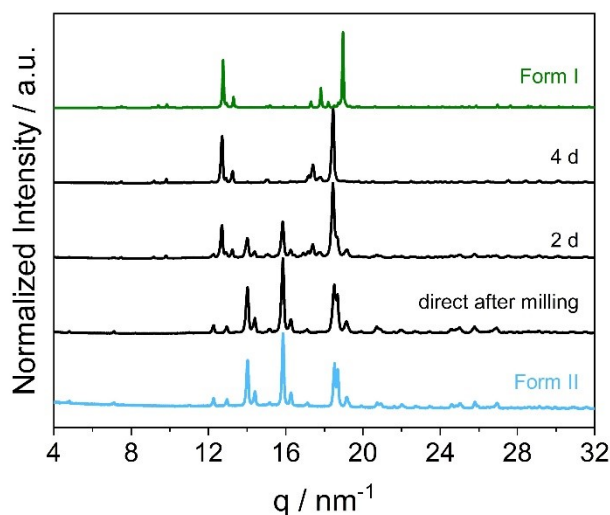


Figure S2.2 | Investigation metastability of **Form I** (measurement directly after the ball milling experiment, after 2 days and after 4 days). The polymorph **Form II** is show below and **Form I** above. We note the offset between simulated and experimental PXRD profiles is the result of measurement temperatures. While simulated data for **Form I** were collected at 153 K², our data were collected at room temperature. By accounting for thermal expansion, a good quality Rietveld refinement is achieved, see Figure S2.1.

To assess the stability of the two polymorphs more accurately, slurry experiments were done in a series of solvent: 1) a polar aprotic solvent, acetonitrile; 2) a polar protic solvent, ethanol; and 3) an apolar solvent, cyclohexane. In each solvent a powder mixture was slurried for 72 h prior to analysis. All the slurries led to formation of **Form I**, Figure S2.3. Pure **Form I** could only

be achieved with acetonitrile. Traces of **Form II** were still present with cyclohexane. These results strongly suggest that **Form I** is thermodynamically stable under ambient conditions.

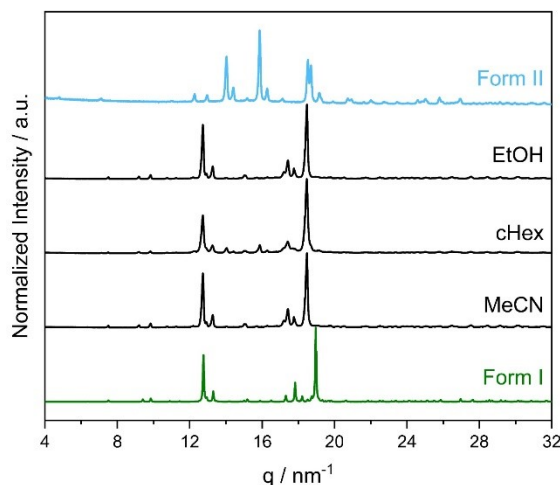


Figure S2.3 | Slurry experiments with a ratio 1:1 (**Form I:Form II**) performed in acetonitrile (MeCN), cyclohexane (cHex) and ethanol (EtOH). Simulated PXRD pattern for **Form I** and **Form II** are given below and above. We note the offset between simulated and experimental PXRD profiles is the result of measurement temperatures. While simulated data for **Form I** were collected at 153 K², our data were collected at room temperature. By accounting for thermal expansion, a good quality Rietveld refinement is achieved, see Figure S2.1.

We simulate the Helmholtz free energy for each of the polymorphic forms at PBEsol-TS level of theory. Simulations were performed with the fully optimized unit cell (*i.e.* the 0 K structure). **Form II** was found to be most stable at temperatures below 130 K, with **Form I** becoming more stable above this temperature, Figure S2.4. We note that we have not accounted for the effects of thermal expansion. However, this ambient temperature stability ordering is consistent with experimental results, *i.e.* that **Form I** is the thermodynamically stable phase at ambient temperature.

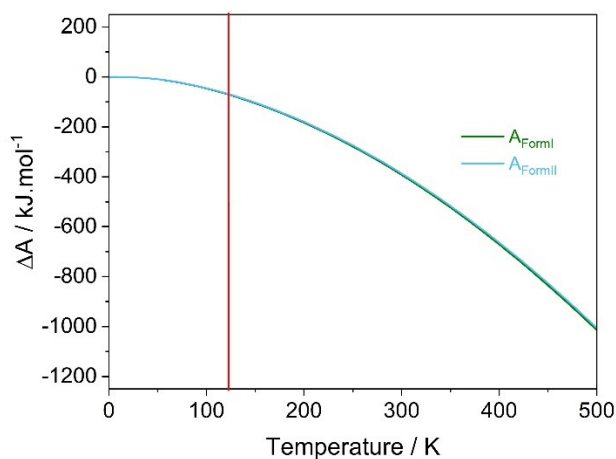
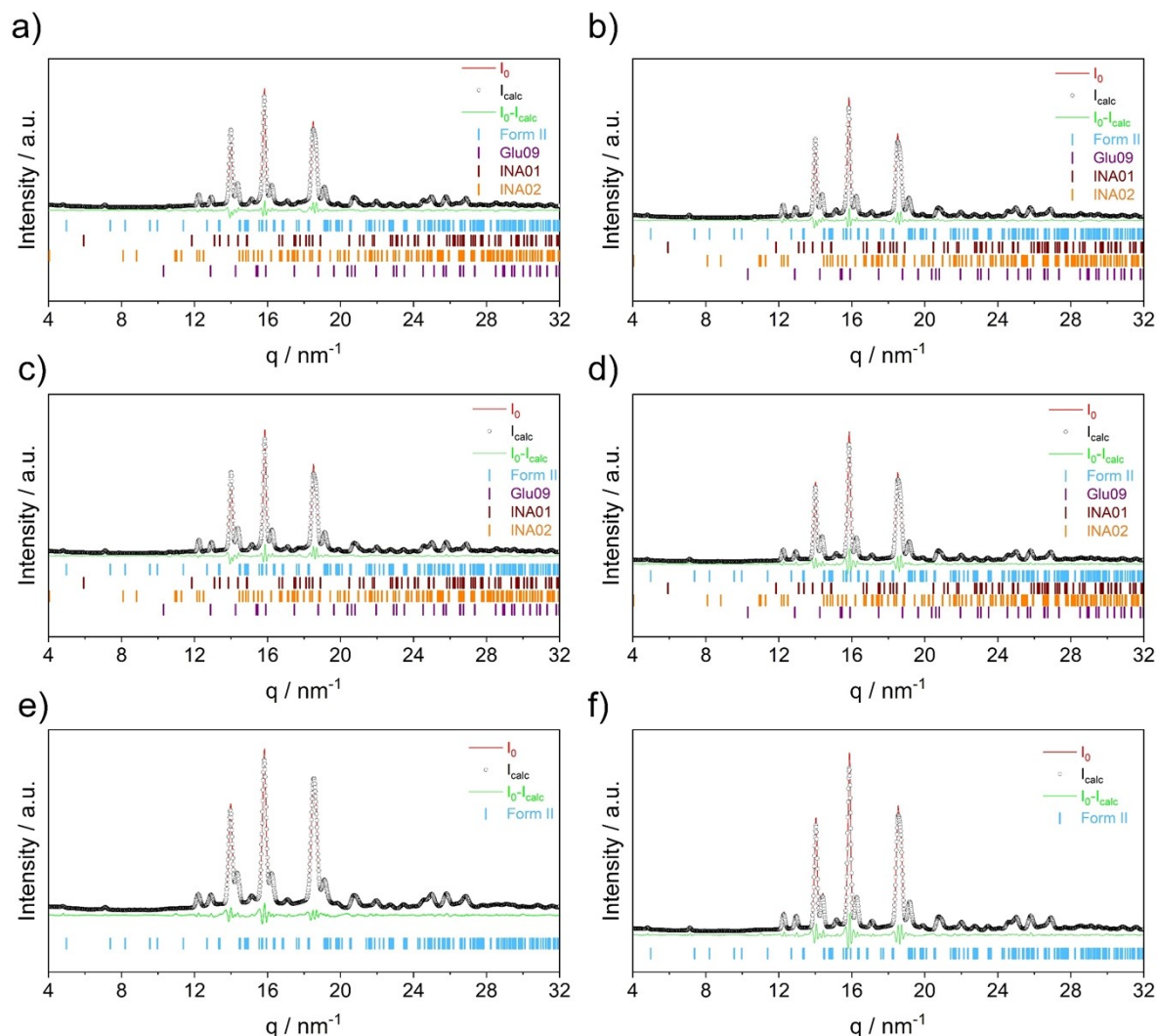


Figure S2.4 | Simulated Helmholtz free energy (A) of **Form I** (green) and **Form II** (blue) form 0-500K. The change of the stability is marked with a vertical red line at 130 K.

S3 Quantitative Phase Analysis of Mechanochemically Prepared Powders

To determine the composition of powder from ball milling experiments, Rietveld refinement was performed for a quantitative phase analysis. The table with the Phase composition for each milling condition and the crystallite size of **Form II** or **Form I** can be found under the respective Rietveld refinement Figure (ambient temperature: Figure S3.1-S3.3 and Table S3.1-S3.3 and at 353 K Figure S3.4-S4.6 and Table S3.4-S3.6).



Fig

Figure S3.1 Results of the phase analyses of INA:GLU with a ball size of 10 mm and a frequency of 50 Hz at ambient temperature: a) at a grinding time of 15 min ($R_{wp} = 6.343$); b) at a grinding time of 30 min ($R_{wp} = 6.642$); c) at a grinding time of 1 h ($R_{wp} = 6.482$); d) at a grinding time of 2 h ($R_{wp} = 7.989$), e) at a grinding time of 5 h ($R_{wp} = 5.770$) and f) at a grinding time of 10 h ($R_{wp} = 7.524$).

Table S3.1 Results of the Rietveld quantitative phase analyses for cocrystal system synthesis using a 10 mm milling ball and a frequency of 50 Hz at ambient temperature. The weighted R -factor (R_{wp}) is given alongside the crystal sizes (CS) obtained from the Scherrer equation.

time	Reagents / %	Form I / %	Form II / %	R_{wp}	CS (Form II) / nm	CS (Form I) / nm
15 min	6	0	94	6.343	39.23	-
30 min	5	0	95	6.642	42.88	-
1 h	7	0	93	6.482	42.10	-
2 h	0	0	100	7.989	42.30	-
5 h	0	0	100	5.770	37.58	-
10 h	0	0	100	7.524	41.75	-

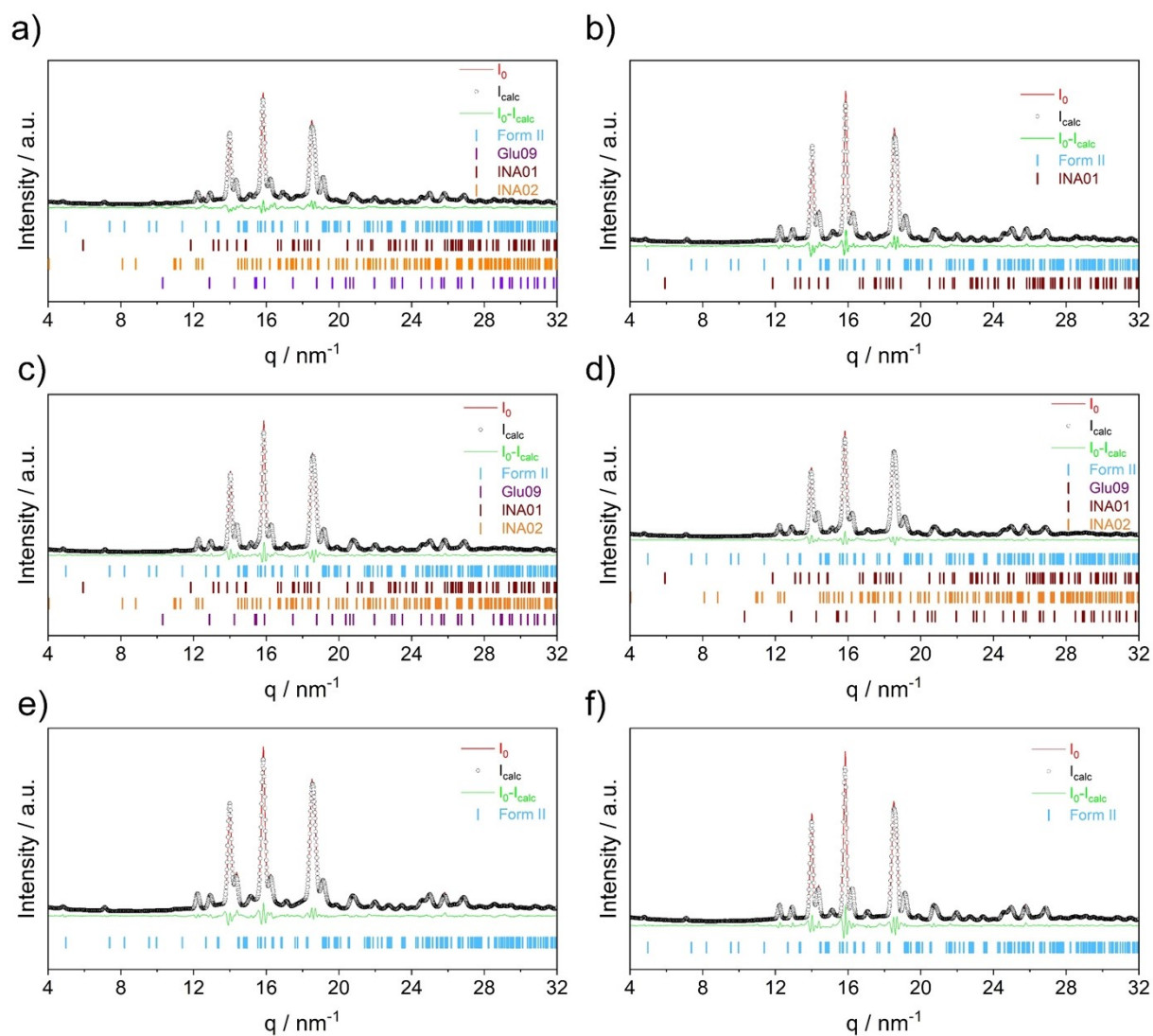


Figure S3.2 Results of the phase analyses of the System INA:GLU with a ball size of 10 mm and a frequency of 35 Hz at ambient temperature: a) at a grinding time of 15 min ($R_{wp} = 6.307$); b) at a grinding time of 30 min ($R_{wp} = 6.731$); c) at a grinding time of 1 h ($R_{wp} = 6.231$); d) at a grinding time of 2 h ($R_{wp} = 5.392$), e) at a grinding time of 5 h ($R_{wp} = 5.726$) and f) at a grinding time of 10 h ($R_{wp} = 7.791$).

Table S3.2 Results of the Rietveld quantitative phase analyses for cocrystal system synthesis using a 10 mm milling ball and a frequency of 35 Hz at ambient temperature. The weighted R -factor (R_{wp}) is given alongside the crystal sizes (CS) obtained from the Scherrer equation.

time	Reagents /%	Form I / %	Form II / %	R_{wp}	CS (Form II) / nm	CS (Form I) / nm
15 min	12	0	88	6.307	35.05	-
30 min	2	0	98	6.731	35.22	-
1 h	8	0	92	6.231	39.53	-
2 h	6	0	94	5.392	39.53	-
5 h	0	0	100	5.726	37.46	-
10 h	0	0	100	7.791	40.86	-

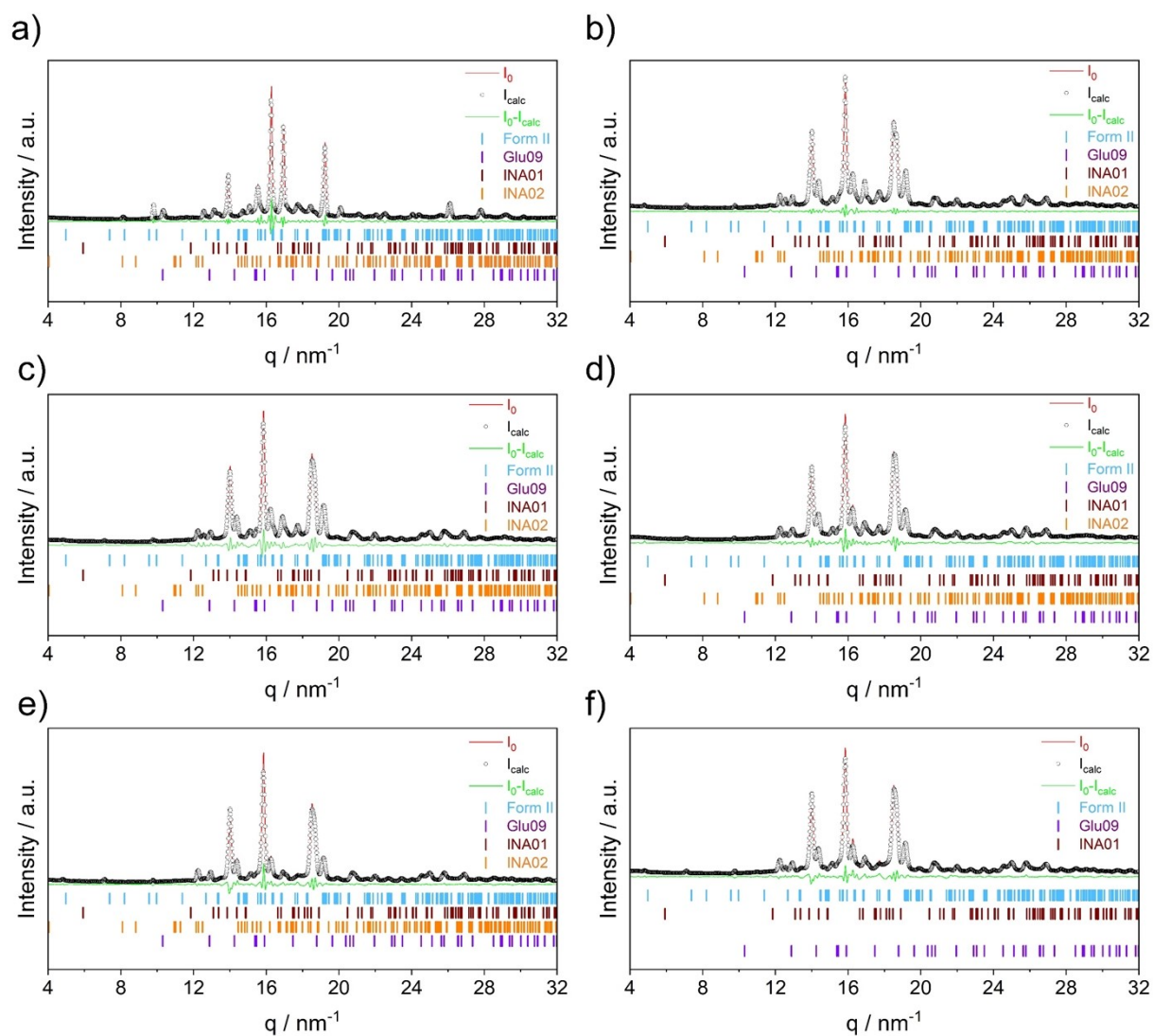


Figure S3.3 Results of the phase analyses of the System INA:GLU with a ball size of 10 mm and a frequency of 20 Hz at ambient temperature: a) at a grinding time of 15 min ($R_{wp} = 7.945$); b) at a grinding time of 30 min ($R_{wp} = 5.566$); c) at a grinding time of 1 h ($R_{wp} = 7.959$); d) at a grinding time of 2 h ($R_{wp} = 6.491$), e) at a grinding time of 5 h ($R_{wp} = 7.480$) and f) at a grinding time of 10 h ($R_{wp} = 6.564$).

Table S3.3 Results of the Rietveld quantitative phase analyses for cocrystal system synthesis using a 10 mm milling ball and a frequency of 20 Hz at ambient temperature. The weighted R -factor (R_{wp}) is given alongside the crystal sizes (CS) obtained from the Scherrer equation.

time	Reagents / %	Form I / %	Form II / %	R_{wp}	CS (Form II) / nm	CS (Form I) / nm
15 min	95	0	5	7.945	-	-
30 min	33	0	67	5.566	42.43	-
1 h	17	0	83	7.959	39.42	-
2 h	12	0	88	6.491	36.17	-
5 h	11	0	89	7.480	44.79	-
10 h	6	0	94	6.564	39.85	-

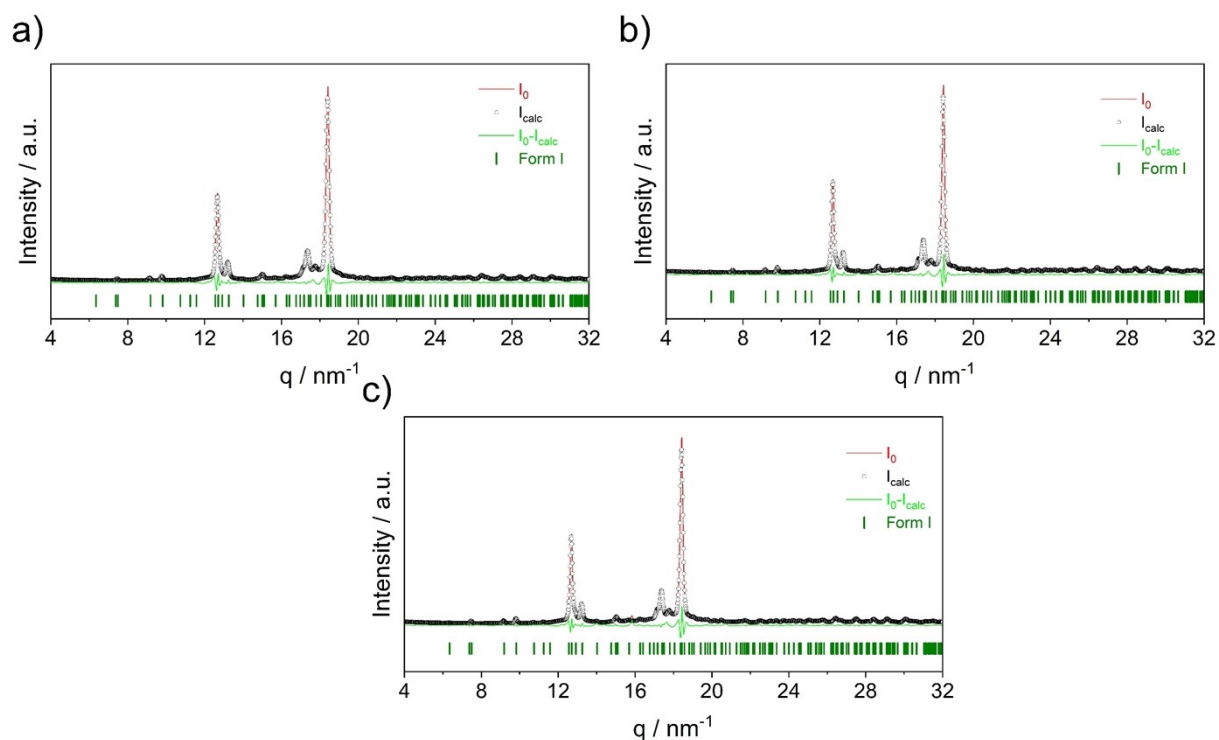


Figure S3.4 | Results of the phase analyses of the System INA:GLU with a ball size of 10 mm and a frequency of 50 Hz at a temperature of 353 K: a) at a grinding time of 1 h ($R_{wp} = 7.74$); b) at a grinding time of 2 h ($R_{wp} = 8.050$); and c) at a grinding time of 5 h ($R_{wp} = 8.851$).

Table S3.4 | Results of the Rietveld quantitative phase analyses for cocrystal system synthesis using a 10 mm milling ball and a frequency of 50 Hz at a temperature of 353 K. The weighted R -factor (R_{wp}) is given alongside the crystal sizes (CS) obtained from the Scherrer equation.

<i>time</i>	Reagents /%	Form I / %	Form II / %	R_{wp}	CS (Form II) / nm	CS (Form I) / nm
1 h	0	100	0	7.740	-	45.23
2 h	0	100	0	8.050	-	55.13
5 h	0	100	0	8.851	-	54.64

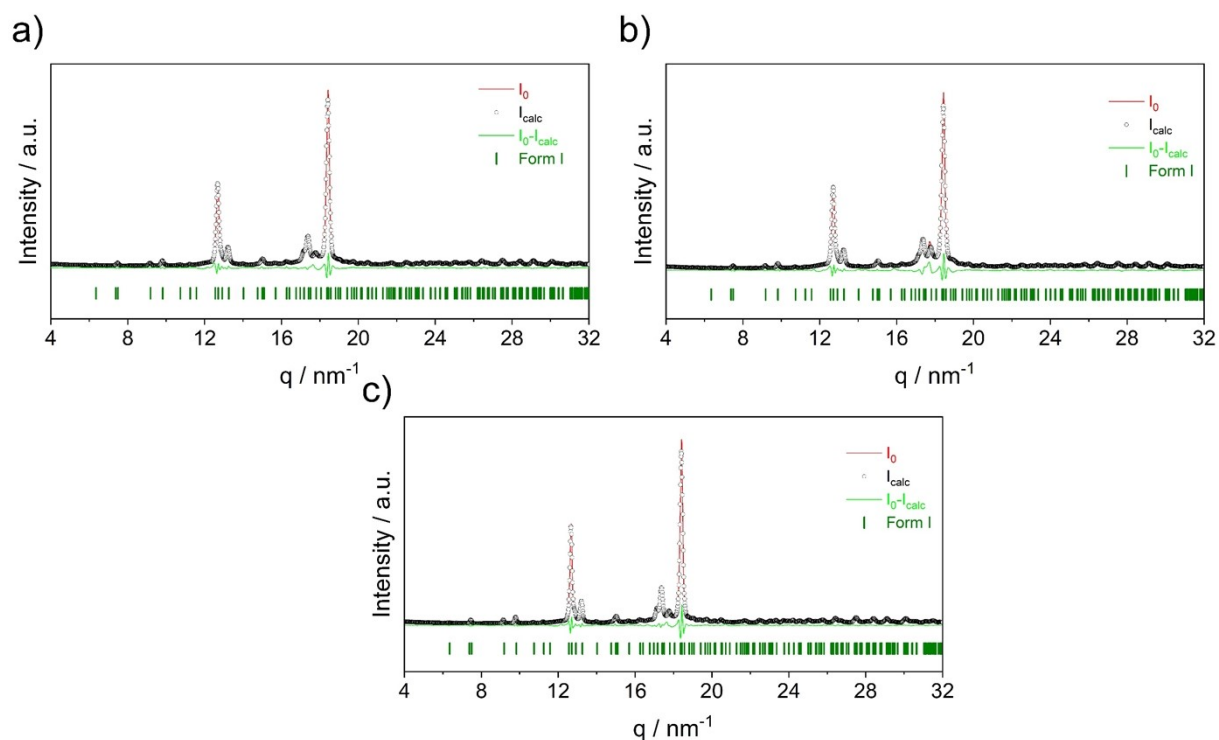


Figure S3.5 Results of the phase analyses of the System INA:GLU with a ball size of 10 mm and a frequency of 35 Hz at a temperature of 353 K: a) at a grinding time of 1 h ($R_{wp} = 6.910$); b) at a grinding time of 2 h ($R_{wp} = 9.081$); and c) at a grinding time of 5 h ($R_{wp} = 7.362$).

Table S3.5 Results of the Rietveld quantitative phase analyses for cocrystal system synthesis using a 10 mm milling ball and a frequency of 35 Hz at a temperature of 353 K. The weighted R -factor (R_{wp}) is given alongside the crystal sizes (CS) obtained from the Scherrer equation.

<i>time</i>	Reagents /%	Form I / %	Form II / %	R_{wp}	CS (Form II) / nm	CS (Form I) / nm
1 h	0	100	0	6.910	-	44.76
2 h	0	100	0	9.081	-	44.23
5 h	0	100	0	7.362	-	60.66

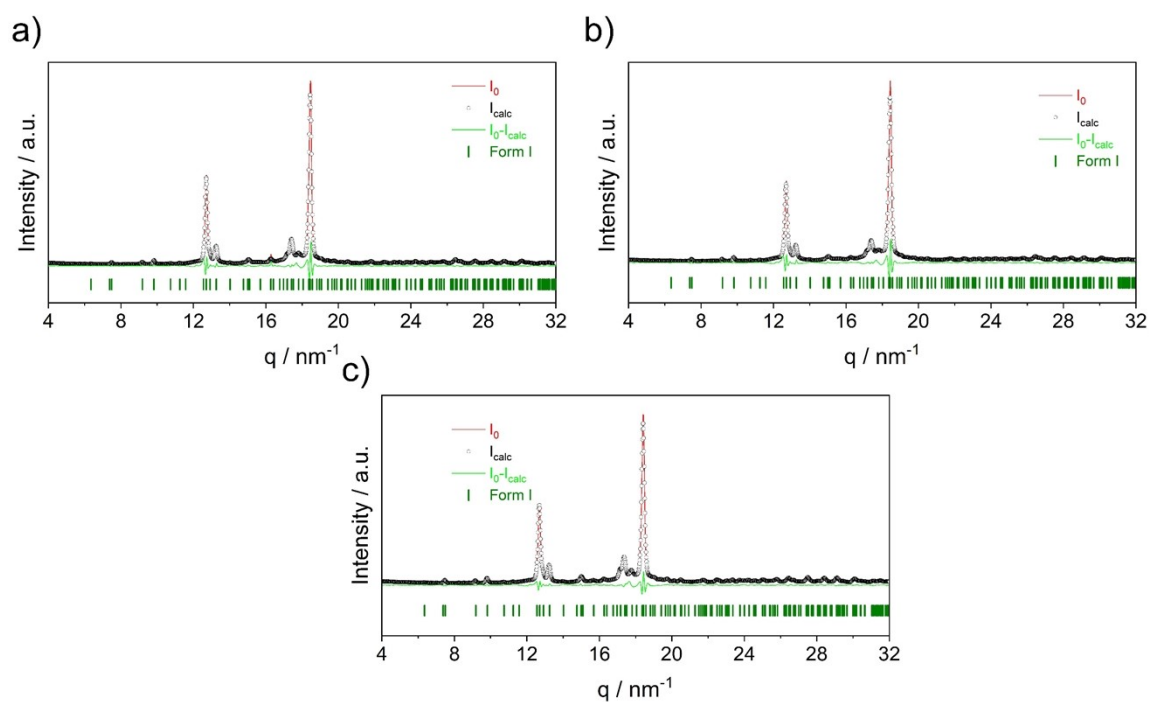


Figure S3.6 | Results of the phase analyses of the System INA:GLU with a ball size of 10 mm and a frequency of 20 Hz at a temperature of 353 K: a) at a grinding time of 1 h ($R_{wp} = 9.040$); b) at a grinding time of 2 h ($R_{wp} = 8.930$); and c) at a grinding time of 5 h ($R_{wp} = 6.839$).

Table S3.6 | Results of the Rietveld quantitative phase analyses for cocrystal system synthesis using a 10 mm milling ball and a frequency of 20 Hz at a temperature of 353 K. The weighted R -factor (R_{wp}) is given alongside the crystal sizes (CS) obtained from the Scherrer equation.

<i>time</i>	Reagents /%	Form I / %	Form II / %	R_{wp}	CS (Form II) / nm	CS (Form I) / nm
1 h	0	100	0	9.040	-	54.82
2 h	0	100	0	8.930	-	49.78
5 h	0	100	0	6.839	-	46.21

S4 Time-Resolved In Situ (TRIS) XRPD

To better understand the mechanism, the mechanochemical experiments were monitored using Time-Resolved *In Situ* (TRIS) PXRD, Figure S4.1 at ambient temperature with three different frequencies (50 Hz, 35 Hz, and 20 Hz) with one stainless milling ball size of 10 mm. It can be observed that with low intensity it takes longer for the reaction to start.

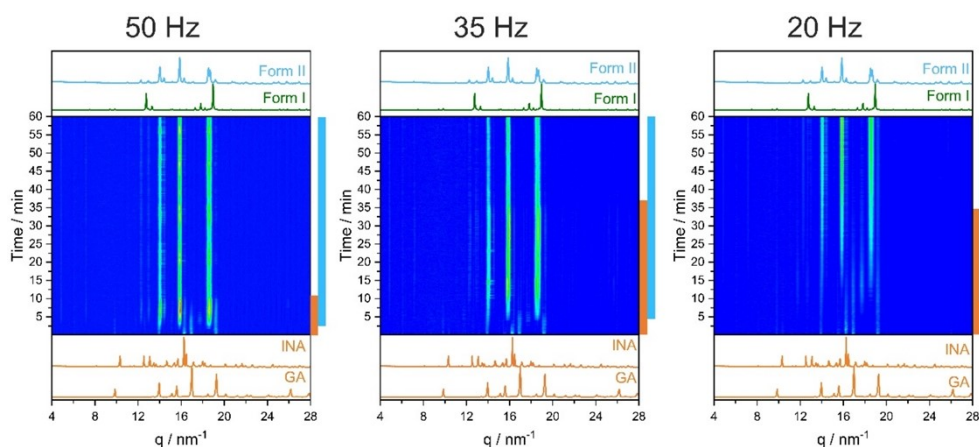


Figure S4.1 Time-Resolved *In Situ* (TRIS) PXRD measurements of the mechanochemical cocrystal formation of INA:GLU using a ball size of 10 mm and three frequencies: 50 Hz (left), 35 Hz (middle), and 20 Hz (right). The experiments were performed at ambient temperature. The diffraction patterns of the starting materials and each product are shown below and above, respectively. The colours mark which phases are present in each step (starting materials: orange and **Form II**: blue). The presence of the colour from **Form II** shows the end of the induction period.

Ball milling at different temperature can be also used to control the interconversion of polymorphic forms under milling conditions. When **Form I** is milled at room temperature (50 Hz, 10 mm ball), it converts to **Form II**, albeit more slowly than nucleation of **Form II** from the starting materials (see Figure S4.2a compared with Figure S4.1). Moreover, milling **Form II** at 353 K (50 Hz, 10 mm ball) for 1 h leads to pure **Form I**, Figure S4.2b.

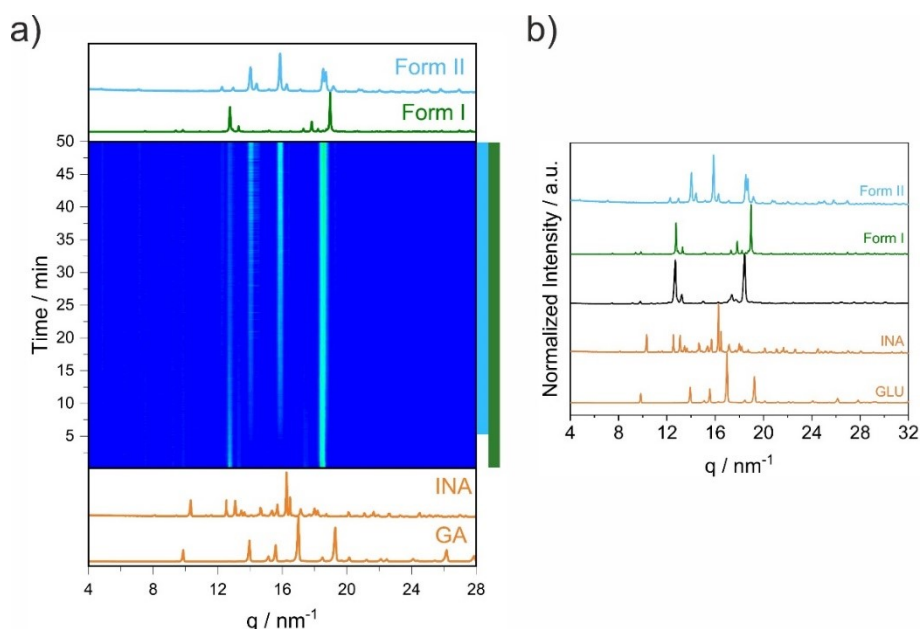


Figure S4.2 Phase transformation of **Form I** to **Form II** a) Time-resolved *in situ* (TRIS) PXRD measurements at room temperature of ball milling of **Form I** using a ball size of 10 mm and a frequency of 50 Hz, showing its conversion to **Form II**. The diffraction patterns of the starting materials and each product are shown below and above, respectively. The colours mark which phases are present in each step (**Form I**: green and **Form II**: blue). b) Results of the milling experiments at 353 K for **Form II**. Milling was performed at 50 Hz with a milling ball size of 10 mm. We note the offset between simulated and experimental XRPD profiles is the result of measurement temperatures. While simulated data for **Form I** were collected at 153 K, our data were collected at room temperature. By accounting for thermal expansion, a good quality Rietveld refinement is achieved, see Figure S2.1.

S5 Ball Milling Experiments at Elevated Temperature

To determine when **Form I** can be obtained, ball milling experiments were carried out from a temperature range of 313-353 K with a ball size of 10 mm and a frequency of 50 Hz, 35 Hz, and 20 Hz (Ball milling experiments at 313 K: Figure S5.1, 323 K: Figure S5.2, 333 K: Figure S5.3, 337 K: Figure S5.4, 343 K: Figure S5.5, 345 K: Figure S5.6, 348 K: Figure S5.7, and 353 K: Figure S5.8; Table S5.1). Ball milling experiments performed within a temperature range of 313-323 K led to **Form II** even after 2 h. No traces of **Form I** could be observed. At a temperature range between 333-345 K the outcoming polymorph become increasingly stochastic. Most of the ball milling experiments lead to the formation of **Form I**. Repeating the ball milling experiments under the same milling conditions could lead to the formation of **Form II**. From a temperature range of 348-353 K, **Form I** could be obtained under all investigated conditions. No traces of **Form II** could be observed.

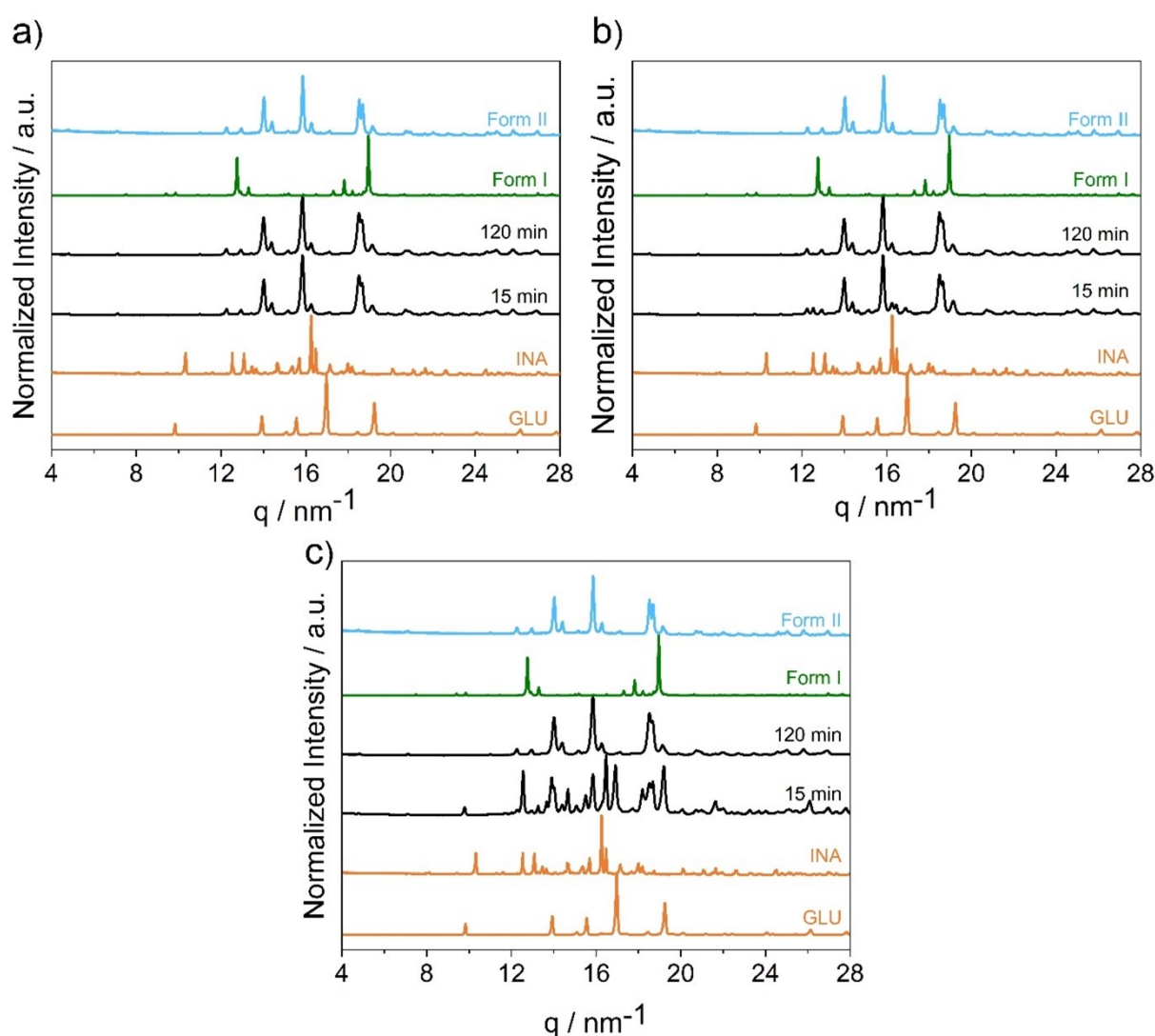


Figure S5.1 Results of the milling experiments at a temperature of 313 K for the cocrystal INA:GLU with a milling ball of 10 mm at a frequency of a: 50 Hz, b: 35 Hz, and c: 20 Hz. We note the offset between simulated and experimental XRPD profiles is the result of measurement temperatures. While simulated data for **Form I** were collected at 153 K², our data were collected at room temperature. By accounting for thermal expansion, a good quality Rietveld refinement is achieved, see Figure S2.1.

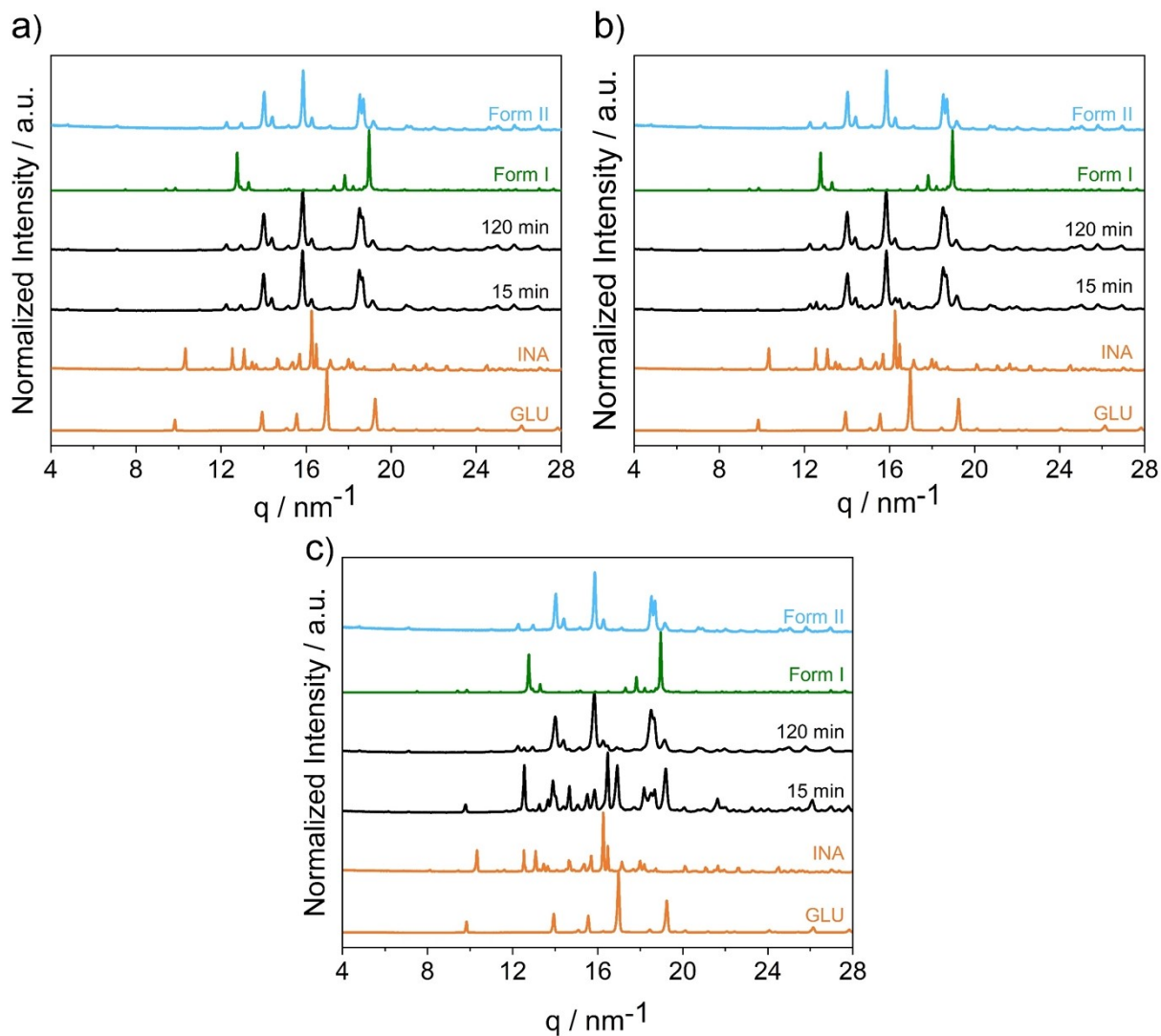


Figure S5.2| Results of the milling experiments at a temperature of 323 K for the cocrystal INA:GLU with a milling ball of 10 mm at a frequency of a: 50 Hz, b: 35 Hz, and c: 20 Hz. We note the offset between simulated and experimental XRPD profiles is the result of measurement temperatures. While simulated data for **Form I** were collected at 153 K², our data were collected at room temperature. By accounting for thermal expansion, a good quality Rietveld refinement is achieved, see Figure S2.1.

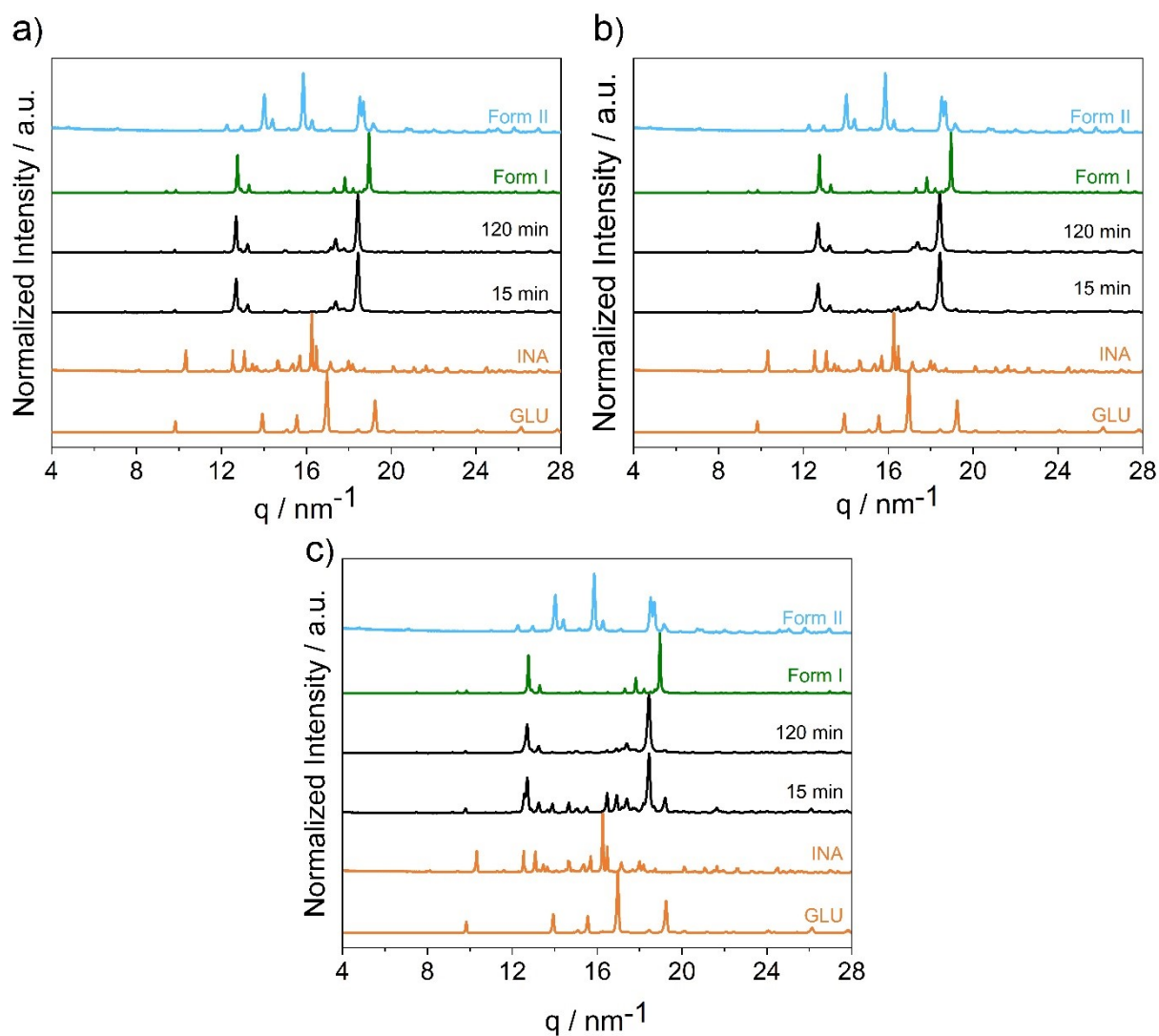


Figure S5.3| Results of the milling experiments at a temperature of 333 K for the cocrystal INA:GLU with a milling ball of 10 mm and a frequency of a: 50 Hz, b: 35 Hz and c: 20 Hz. We note the offset between simulated and experimental XRPD profiles is the result of measurement temperatures. While simulated data for **Form I** were collected at 153 K², our data were collected at room temperature. By accounting for thermal expansion, a good quality Rietveld refinement is achieved, see Figure S2.1.

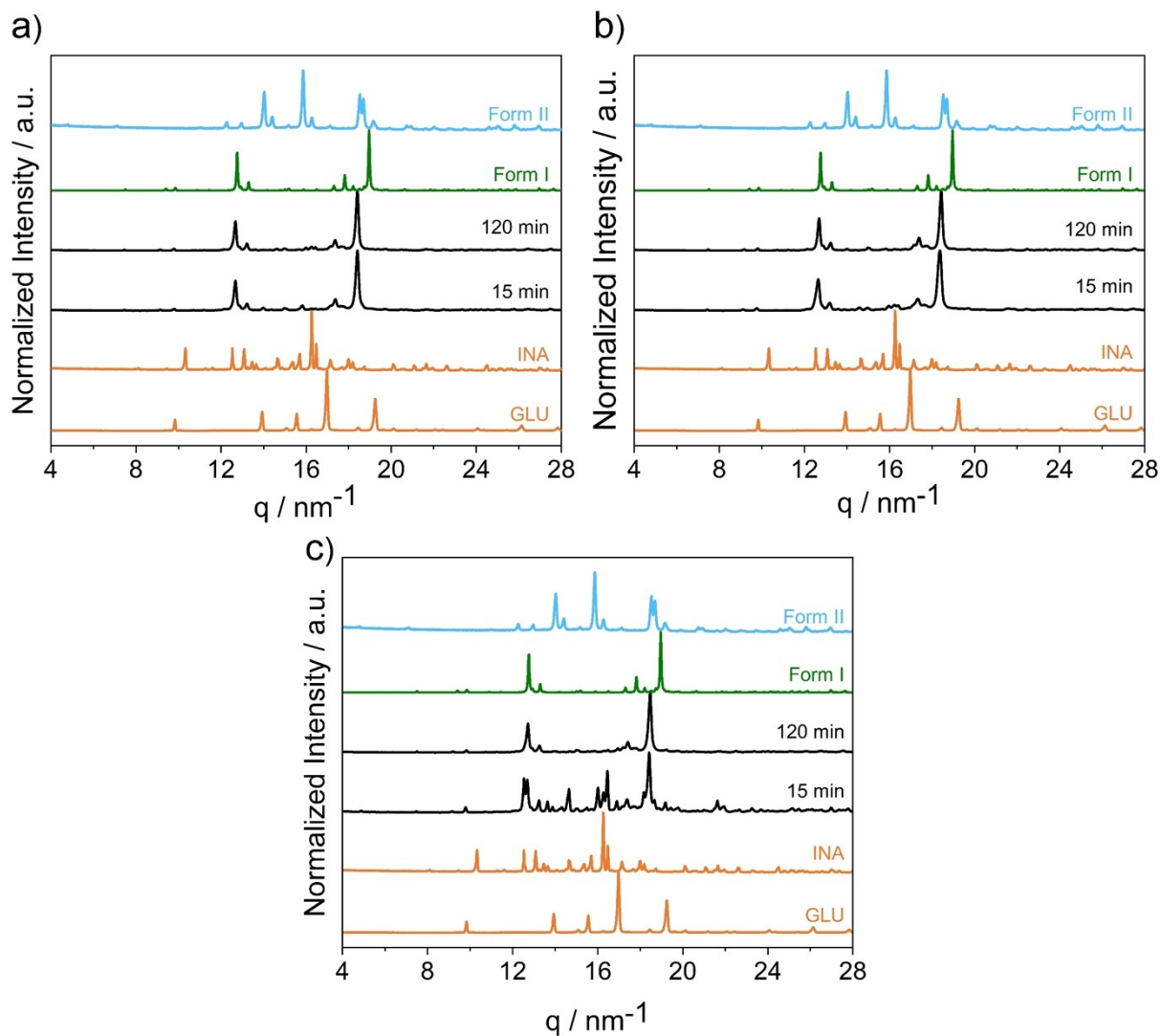


Figure S5.4| Results of the milling experiments at a temperature of 337 K for the cocrystal INA:GLU with a milling ball of 10 mm and a frequency of a: 50 Hz, b: 35 Hz, and c: 20 Hz. We note the offset between simulated and experimental XRPD profiles is the result of measurement temperatures. While simulated data for **Form I** were collected at 153 K², our data were collected at room temperature. By accounting for thermal expansion, a good quality Rietveld refinement is achieved, see Figure S2.1.

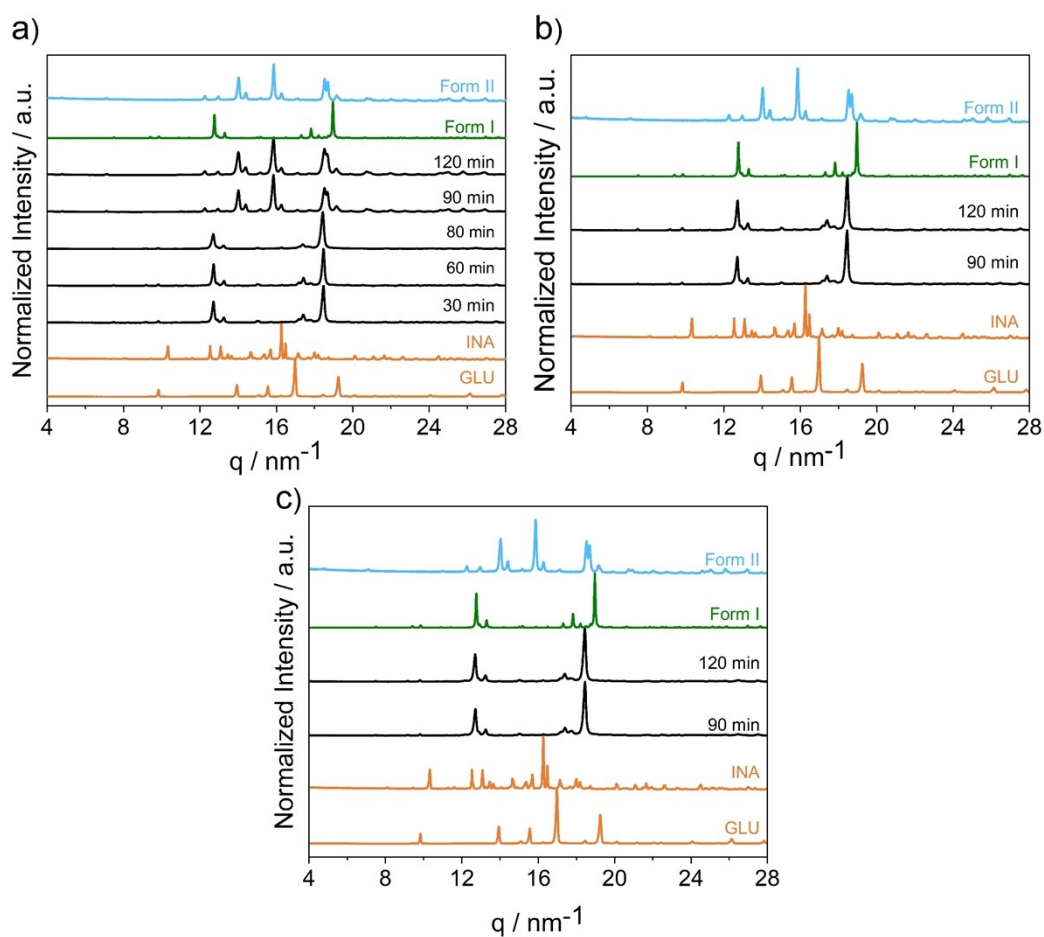


Figure S5.5| Results of the milling experiments at a temperature of 343 K for the cocystal INA:GLU with a milling ball of 10 mm and a frequency of a: 50 Hz, b: 35 Hz and c: 20 Hz. We note the offset between simulated and experimental XRPD profiles is the result of measurement temperatures. While simulated data for **Form I** were collected at 153 K², our data were collected at room temperature. By accounting for thermal expansion, a good quality Rietveld refinement is achieved, see Figure S2.1.

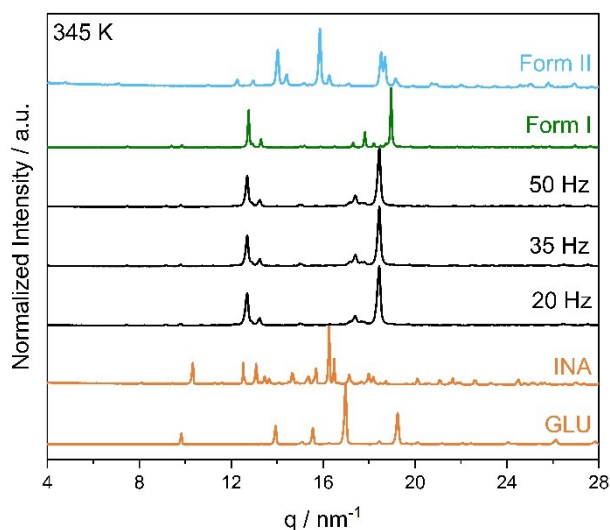


Figure S5.6| Results of the milling experiments at a temperature of 345 K for the cocystal INA:GLU at three different frequencies (50 Hz, 35 Hz, and 20 Hz) with a milling ball size of 10 mm for 2 h. We note the offset between simulated and experimental XRPD profiles is the result of measurement temperatures. While simulated data for **Form I** were collected at 153 K², our data were collected at room temperature. By accounting for thermal expansion, a good quality Rietveld refinement is achieved, see Figure S2.1.

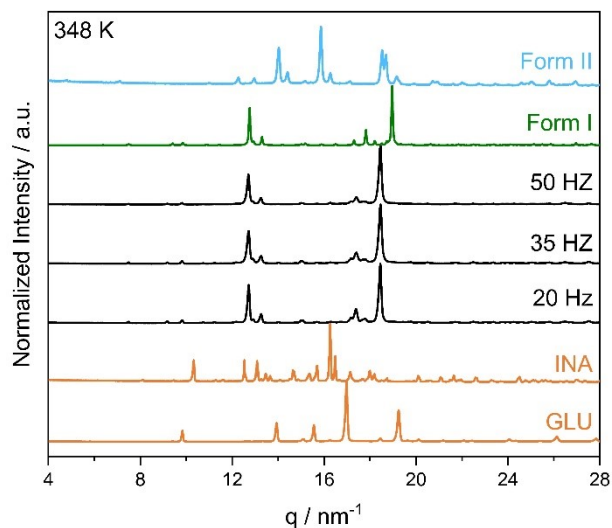


Figure S5.7 | Results of the milling experiments at a temperature of 348 K for the cocrystal INA:GLU at three different frequencies (50 Hz, 35 Hz, and 20 Hz) with a milling ball size of 10 mm for 2 h. We note the offset between simulated and experimental XRPD profiles is the result of measurement temperatures. While simulated data for **Form I** were collected at 153 K², our data were collected at room temperature. By accounting for thermal expansion, a good quality Rietveld refinement is achieved, see Figure S2.1.

Table S5.1 | Formation of **Form I** and **Form II** at different temperatures (room temperature, 333 K, 337 K, 343 K, 345 K, and 348 K) with a frequency of 50 Hz, 35 Hz and 20 Hz and one stainless steel ball with a ball size of 10 mm. Each entry in the table corresponds to a separate experiment.

Temperature / K	Frequency / Hz		
	50	35	20
313	Form II (15 min)	Form II (15 min)	Form II (15 min)
	Form II (120 min)	Form II (120 min)	Form II (120 min)
323	Form II (15 min)	Form II (15 min)	Form II (15 min)
	Form II (120 min)	Form II (120 min)	Form II (120 min)
333	Form I or Form II (15 min)	Form I (15 min)	Form I (15 min)
	Form I or Form II (120 min)	Form I (120 min)	Form I (120 min)
337	Form I and traces of Form II (15 min)	Form I (15 min)	Form I (15 min)
	Form I (120 min)	Form I (120 min)	Form I (120 min)
	Form I (30 min)		
343	Form I (80 min)	Form I (90 min)	Form I (90 min)
	Form I (85 min)	Form I (120 min)	Form I (120 min)
	Form II (95%) + Form I (5%) 90 min		
	Form I or Form II 120 min		
345	Form I (120 min)	Form I (120 min)	Form I (120 min)
348	Form I (120 min)	Form I (120 min)	Form I (120 min)

Ball milling experiments at 353 K were done at three different frequencies (50 Hz, 35 Hz, and 20 Hz) using one stainless steel ball (diameter 10 mm, mass 4.04 ± 0.02 g), Figure S5.8. Under all milling conditions neat grinding a stoichiometric mixture of INA and GLU (Figure 5.8b, orange) lead to formation of pure **Form I**. No traces of **Form II** could be observed. The highest investigated energy milling experiments (50 Hz, 10 mm, $2.03 \text{ mJ}\cdot\text{Imp}^{-1}$) and the lowest (20 Hz, 10 mm, $0.32 \text{ mJ}\cdot\text{Imp}^{-1}$) led to pure **Form I**, which is stable for 5 h, Figure S5.8b. Similar to milling experiments under ambient temperature, the energy input has no effect obtained polymorph. Like the formation of **Form II** at ambient temperature, the crystallize size of **Form I** is constant over the selected experiment duration, Figure S5.8c.

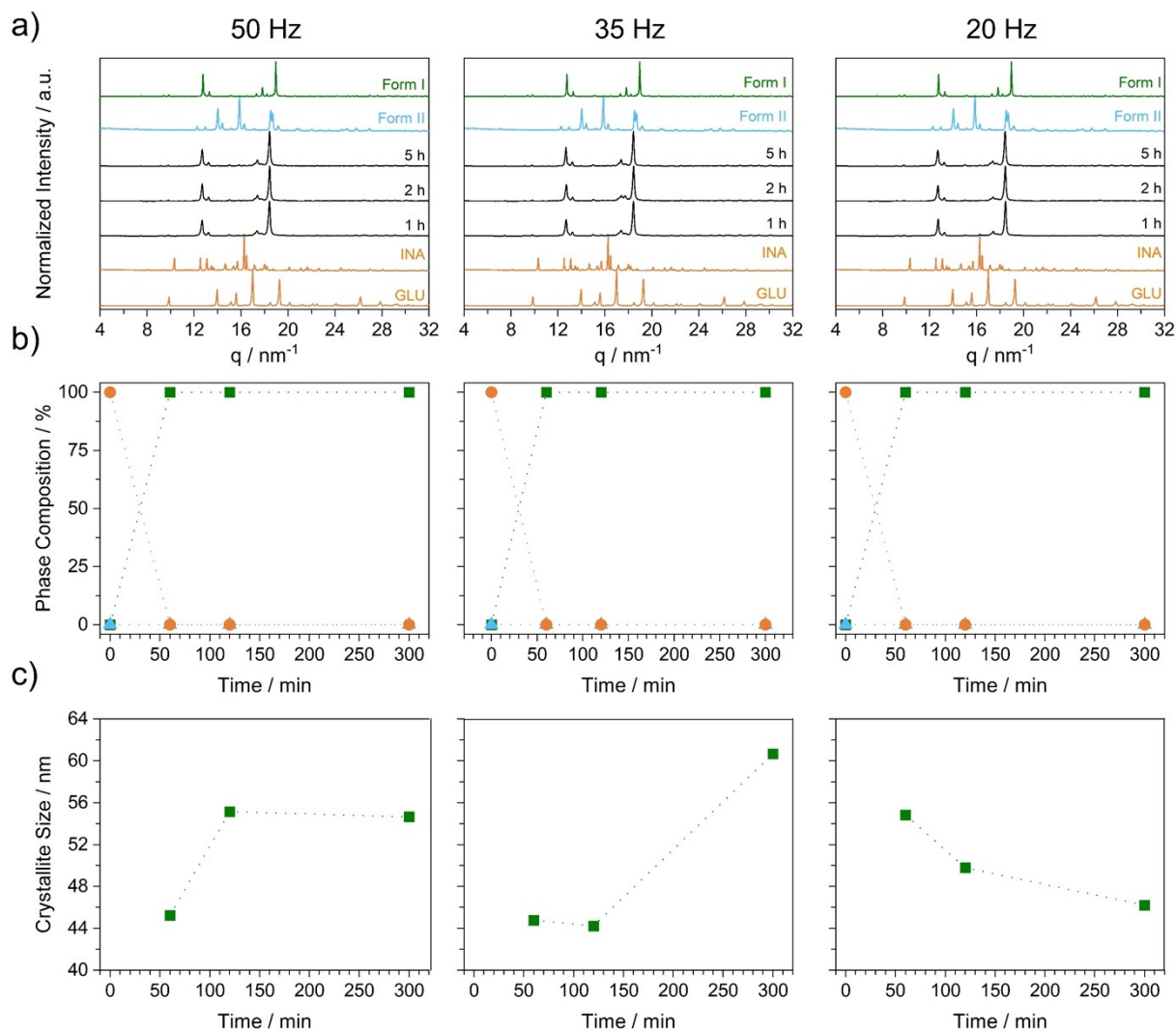


Figure S5.8 | Results of the milling experiments at a temperature of 353 K for the cocrystal INA:GLU at 50 Hz (left), 35 Hz (middle), and 20 Hz (right) with a milling ball size of 10 mm. a) PXR pattern with the diffraction patterns of the starting materials (orange) and **Form I** (green) and **Form II** (blue) are given below and above. b) Phase composition of the milling experiments: sum of INA and GLU (orange circle), **Form I** (green square) and **Form II** (blue triangle). c) Evolution of the crystallite size of **Form I** (green square).

S6 REFERENCES

- 1 G. I. Lampronti, A. A. L. Michalchuk, P. P. Mazzeo, A. M. Belenguer, J. K. M. Sanders, A. Bacchi and F. Emmerling, *Nat Commun*, 2021, **12**, 6134.
- 2 P. Vishweshwar, A. Nangia and V. M. Lynch, *Crystal Growth & Design*, 2003, **3**, 783–790.